University of Wollongong

Research Online

1-1-2016

A high-performance rechargeable Mg2+/Li+ hybrid battery using one-dimensional mesoporous TiO2(B) nanoflakes as the cathode

Shuojian Su
Shanghai Jiao Tong University

Yanna Nuli
Shanghai Jiao Tong University, yanna@uow.edu.au

Zhenguo Huang
University of Wollongong, zhenguo@uow.edu.au

Qi Miao
Shanghai Jiao Tong University

Jun Yang
Shanghai Jiao Tong University, yangj723@sjtu.edu.cn

See next page for additional authors

Follow this and additional works at: https://ro.uow.edu.au/aiimpapers

Part of the Engineering Commons, and the Physical Sciences and Mathematics Commons

Recommended Citation

A high-performance rechargeable Mg2+/Li+ hybrid battery using one-dimensional mesoporous TiO2(B) nanoflakes as the cathode

Abstract

Mg2+/Li+ hybrid batteries have recently been constructed combining a Mg anode, a Li+-intercalation electrode, and an electrolyte containing both Mg2+ and Li+. These batteries have been reported to outperform all the previously reported magnesium batteries in terms of specific capacity, cycling stability, and rate capability. Herein, we report the outstanding electrochemical performance of Mg2+/Li+ hybrid batteries consisting of a one-dimensional mesoporous $TiO_2(B)$ cathode, a Mg anode, and an electrolyte consisting of 0.5 mol L-1 Mg(BH4)2 + 1.5 mol L-1 LiBH4 in tetraglyme. A highly synergetic interaction between Li+ and Mg2+ ions toward the pseudo-capacitive reaction is proposed. The hybrid batteries show superior rate performance with 130 mAh g-1 at 1 C and 115 mAh g-1 at 2 C, together with excellent cyclability up to 6000 cycles.

Keywords

b, tio2, high, performance, rechargeable, cathode, mg2, nanoflakes, li, hybrid, battery, one, dimensional, mesoporous

Disciplines

Engineering | Physical Sciences and Mathematics

Publication Details

Authors

Shuojian Su, Yanna Nuli, Zhenguo Huang, Qi Miao, Jun Yang, and Jiulin Wang

A High-performance Rechargeable Mg^{2+}/Li^+ Hybrid Battery Using One-dimensional Mesoporous TiO_2(B) Nanoflakes as the Cathode

Shuojian Su, [a] Yanna NuLi, [a]* Zhenguo Huang, [b]* Qi Miao,[a] Jun Yang [a] and Jiulin Wang [a]

[a] School of Chemistry and Chemical Engineering, Shanghai Electrochemical Energy Devices Research Center, Hirano Institute for Materials Innovation, Shanghai Jiao Tong University, Shanghai 200240, P. R. China. E-mail: nlyn@sjtu.edu.cn

[b] Institute for Superconducting and Electronic Materials, University of Wollongong, Wollongong, NSW 2522, Australia. E-mail: zhenguo@uow.edu.au

KEYWORDS: hybrid batteries, Mg^{2+}/Li^+ hybrid, Mg batteries, TiO_2, borohydride

ABSTRACT. Mg^{2+}/Li^+ hybrid batteries have recently been constructed combining an Mg anode, an Li^+-intercalation electrode, and an electrolyte containing both Mg^{2+} and Li^+. These batteries have been reported to outperform all the previously reported magnesium batteries in terms of specific capacity, cycling stability, and rate capability. Herein, we report the outstanding electrochemical performance of Mg^{2+}/Li^+ hybrid batteries consisting of one-dimensional (1D) mesoporous TiO_2(B) cathode, Mg anode, and an electrolyte consisting of 0.5 mol L^{-1} $Mg(BH_4)_2$+1.5 mol L^{-1} $LiBH_4$ in tetraglyme (TG). A highly synergetic interaction between Li^+

and Mg^{2+} ions toward the pseudo-capacitive reaction is proposed. The hybrid batteries show superior rate performance with 130 mAh g^{-1} at 1 C and 115 mAh g^{-1} at 2 C, together with excellent cycleability up to 6000 cycles.

1. INTRODUCTION

The rechargeable magnesium batteries feature the following competitive advantages: 1) high theoretical volumetric capacity (3832 and 2062 mAh cm^{-3} for Mg and Li, respectively), 2) low costs (currently 24 times cheaper than Li), and 3) high safety (unlike Li metal, Mg can be electrodeposited rather smoothly without dendritic growth).[1, 2] They are therefore promising for both mobile and stationary applications, including electric vehicles and load-leveling electricity storage stations. The intrinsic strong coulombic interactions between bivalent Mg^{2+} ions and the host materials, however, causes sluggish Mg^{2+} diffusion and large polarization, and consequently, low Mg^{2+} intercalation levels and/or rapid capacity decay.[3, 4] To circumvent the issues associated with the intercalation but still take advantage of the high capacity and high safety associated with Mg deposition and dissolution, Mg^{2+}/Li^+ hybrid batteries have recently been constructed combining an Mg anode, an Li^+-intercalation electrode, and an electrolyte containing both Mg^{2+} and Li^+.[5-10] These batteries have been reported to outperform all the previously reported magnesium batteries in terms of specific capacity, cycling stability, and rate capability.

Two key aspects have to be carefully examined when designing the Mg^{2+}/Li^+ hybrid batteries, i.e., the electrolyte and the cathode. The anodic stability of Mg^{2+}/Li^+ electrolyte sometime decreases due to the reaction between Li and Mg salts.[5] For example, the anodic stability limit of $Mg(AlCl_{4-n}Ph_n)_2$ (all phenyl complex) in tetrahydrofuran (THF) drops to 2.5 V from 3.0 V (*vs.* Mg/Mg^{2+}) when $LiBF_4$ is added, because BF_4^- reacts with PhMgCl to form $B(Ph)_4^-$.[5, 7] Most

recently, $Mg(BH_4)_2$ dissolved in TG, a potentially safer ether solvent, has been used as the electrolyte for rechargeable Mg batteries.[11] The strong chelation arising from the five oxygen atoms per TG molecule results in enhanced dissociation between BH_4^- and Mg^{2+}, and thus, improved Mg deposition-dissolution.[12, 13] $LiBH_4$ was found to be an effective additive to improve the conductivity of the solution while still maintaining the anodic stability. The 0.5 mol L^{-1} $Mg(BH_4)_2$+1.5 mol L^{-1} $LiBH_4$/TG solution demonstrates 2.4 V anodic stability on non-inert stainless steel current collector and nearly 100% coulombic efficiency for reversible Mg deposition and dissolution. This mixed solution displays good compatibility with Mo_6S_8 [11] and TiO_2 cathode [8].

The cathode needs to possess effective Li^+ storage capability and a suitable working voltage that matches the electrochemical window of the electrolyte. Considering the anodic stability of the electrolyte (2.1 V for $Mg(BH_4)_2$+$LiBH_4$/TG) on stainless steel current collector with poly(vinylidene difluoride) (PVDF) binder (The binder also has an influence on the stability of the electrolyte. Figure S1 in the Supporting Information), $TiO_2(B)$ is believed to be a promising candidate due to its high capacity and flat working voltage plateau (about 0.9 V *vs*. Mg) within the electrochemical window. Several key morphological features have been created to enhance the performance of $TiO_2(B)$. For example, nanostructured $TiO_2(B)$ affords stable and high rate charge/discharge capabilities through a surface faradic redox reaction, i.e., the pseudo-capacitive behavior originating from the unique sites and energetics of Li^+ ion absorption and diffusion.[14, 15] 1D $TiO_2(B)$ nanostructures, such as nanowires,[16-19] nanotubes,[20, 21] and hybrid nanostructures,[22, 23] have shown excellent performance because the 1D structure facilitates the electron transport along the elongated dimension and the two short dimensions ensure fast Li^+ insertion-deinsertion.[24] Nanostructured mesoporous TiO_2 (anatase) shows a superior high rate capability

duo to negligible diffusion times, enhanced local conductivities, and possibly faster phase transfer reactions.[25] Mesopores have also been introduced into microsized $TiO_2(B)$ particles to accommodate strain during cycling.[26] Therefore, it is ideal to employ 1D mesoporous $TiO_2(B)$ with these desired properties for Mg^{2+}/Li^+ hybrid batteries.

2. MATERIALS AND METHODS

2. 1 Preparation of TiO_2 (B)

Monoclinic $TiO_2(B)$ was prepared by a hydrothermal process followed by heat-treatment. Commercial fine TiO_2-anatase powders (99.8%, Aldrich) were added to a 10 M NaOH aqueous solution. After a 30-min ultrasound and a 30-min stir, the obtained emulsion was transferred into a 50 mL autoclave, which was then kept in an oven at 180 °C for 72 h. After naturally cooling to room temperature, the resultant white precipitates were isolated from the solution by centrifugation. The powders were washed using 0.1 mol L^{-1} HCl solution and then ion-exchanged in 0.1 mol L^{-1} HCl solution for 4 h to make $H_2Ti_3O_7$.[19] After this, the as-obtained proton-exchanged titanate was washed using deionized water until the pH was 7 and then freeze dried for 20 h. Finally, the dried product was calcined at 400 °C for 4 h to make $TiO_2(B)$ nanoflakes.

2.2 Preparation of electrolyte

The preparation was conducted in an argon-filled glove box (Mbraun, Unilab, Germany) containing less than 2 ppm H_2O and O_2. The 0.5 mol L^{-1} $Mg(BH_4)_2$+1.5 mol L^{-1} $LiBH_4$/TG and the 1.5 mol L^{-1} $LiBH_4$/TG electrolytes were prepared by dissolving the predetermined amounts of $Mg(BH_4)_2$ (Sigma-Aldrich, 95%) and $LiBH_4$ (J&K Scientific, 95%) in tetraglyme (TG) (Aladdin, further dried over 3 Å molecular sieves). 1.0 mol L^{-1} $LiPF_6$ in a mixture of ethylene carbonate (EC) and dimethyl carbonate (DMC) (EC:DMC = 1:1, by volume) was purchased from

Zhangjiagang Guotai Huarong Chemical New Material Co., Ltd. The specific conductivity of the solutions was measured using a DDS-307A conductivity meter (Shanghai Kejin). ^{7}Li nuclear magnetic resonance (NMR) spectra were recorded on a MERCURY plus 400 Nuclear Magnetic Resonance spectrometer (Varian, Inc., USA) while referenced to LiCl dissolved in D_2O.

2.3 Characterization

X-ray diffraction (XRD) measurements were performed on a Rigaku diffractometer D/MAX-2200/PC equipped with Cu Kα radiation (λ = 0.15418 nm). Textural and microtextural characterizations were conducted using scanning electron microscopy (SEM) on a JEOL field-emission microscope (JSM-7401F) and transmission electron microscopy (TEM) on a JEOL high-resolution electron microscope (JEM-2010). N_2 adsorption-desorption experiments were carried out at -196 °C on a ASAP 2010 M+C surface area and pore analyzer (Micromeritics, USA) after degassing the samples at 150-200 °C for 3 h. The *ex situ* Raman spectra were collected at room temperature with a DXR Raman microscope (Thermo Scientific) using a HeNe laser with a wavelength of 532 nm as the excitation source.

2.4 Electrochemical Measurements.

$TiO_2(B)$ cathode slurry was prepared by mixing 70 wt % active material, 20 wt % super-P carbon powder (Timcal), and 10 wt % poly(vinylidene fluoride) (PVDF, dissolved in N-methyl-2-pyrrolidinone). The electrode discs with a diameter of 12 mm were prepared by following these steps: coating the slurry onto a stainless steel foil current collector, drying at 80 °C for 1 h, pressing at 2 MPa, vacuum drying at 100 °C for 4 h, and punching the foil into discs. Polished Mg foil was used as the anode, and CR2016 coin cells were assembled in an argon-filled glove box. Cyclic voltammetry measurements were performed on a CHI650C Electrochemical

Workstation (Shanghai, China). Galvanostatic discharge-charge measurements were conducted at ambient temperature on a Land battery measurement system (Wuhan, China).

3. RESULTS AND DISCUSSION

1D mesoporous $TiO_2(B)$ was prepared via a hydrothermal process followed by heat-treatment. The wide-angle X-ray diffraction (XRD) pattern (Figure 1a) can be indexed to the monoclinic $TiO_2(B)$ phase (JCPDS No. 46-1237). $TiO_2(B)$ can be readily distinguished from the anatase TiO_2 structure by the absence of the peak at 37.8º (004).[27] The well-defined peak in the small-angle XRD pattern (inset in Figure 1a) is indicative of a mesoporous structure, which was later confirmed by high-resolution transmission electron microscopy (HRTEM) observation. Raman spectroscopy was also used, since laboratory XRD is not able to detect minor phases and amorphous matter. The Raman bands (Figure 1b) can be assigned to the vibrations in $TiO_2(B)$.[28-31] Characteristic peaks of anatase TiO_2 at 395 and 515 cm^{-1} are absent,[32, 33] which proves the formation of single phase $TiO_2(B)$. The scanning electron microscope (SEM) image in Figure 1c shows a general view of 1D $TiO_2(B)$, which is made up of nanoflakes with thickness of several tens to hundreds of nanometers and length of 2-4 μm. The TEM image (Figure 1d) reveals the mesoporous nature of the nanoflakes, with the HRTEM image (Figure 1e) indicating a clear hierarchical pore structure in the range of 2-20 nm on the surface. The resolved lattice fringes and fast Fourier transform (FFT) pattern (inset, Figure 1e) confirm the formation of monoclinic $TiO_2(B)$ (Figure S2). The mesoporosity is further confirmed by nitrogen adsorption-desorption analysis, which reveals a typical type IV isotherm (Figure 1f) with a clear H3-type hysteretic loop. The Brunauer-Emmett-Teller (BET) specific surface area is 44.27 cm^2 g^{-1}, and the pore volume is 0.181 cm^3 g^{-1}, which are larger than previously reported.[27] The pore size distribution

obtained using the Barrett-Joyner-Hallenda (BJH) method (inset, Figure 1f) shows two maxima centered at 2 and 11.6 nm, respectively. The formation of mesopores is likely to be due to the water evolution during the thermal conversion from $H_2Ti_3O_7$ to $TiO_2(B)$. The mesopores would enable good contact between the electrolyte and the cathode, and consequently enhance electrochemical reactions.
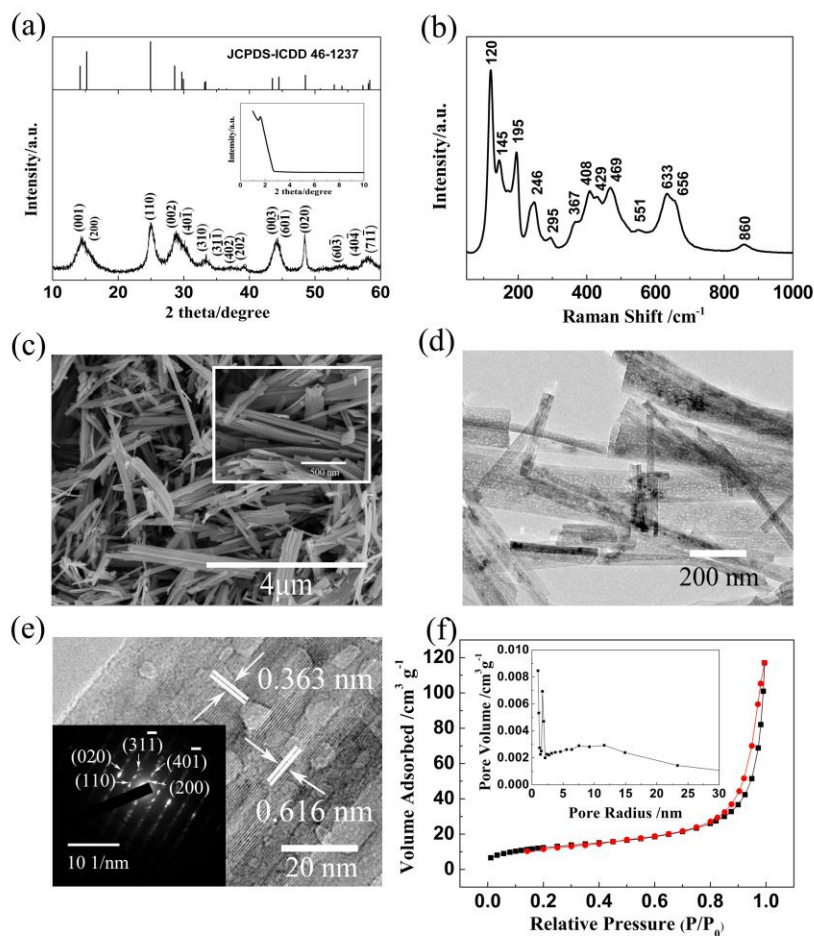
Figure 1. (a) Wide-angle powder X-ray diffraction pattern of the as-prepared $TiO_2(B)$ matches well with the standard pattern (JCPDS No. 46-1237). Small-angle powder X-ray diffraction pattern in the inset indicates its mesoporous nature. (b) Raman spectrum reveals pure $TiO_2(B)$ phase. The SEM image in (c) with a higher magnification in the inset shows the $TiO_2(B)$ nanoflakes. TEM images in (d) and (e) indicate the porous nature of the nanoflakes; both the

lattice fringes (e) and the FFT pattern (inset in (e)) confirm the formation of $TiO_2(B)$. (f) Nitrogen adsorption-desorption isotherm of mesoporous $TiO_2(B)$ nanoflakes. The inset shows the pore size distribution.
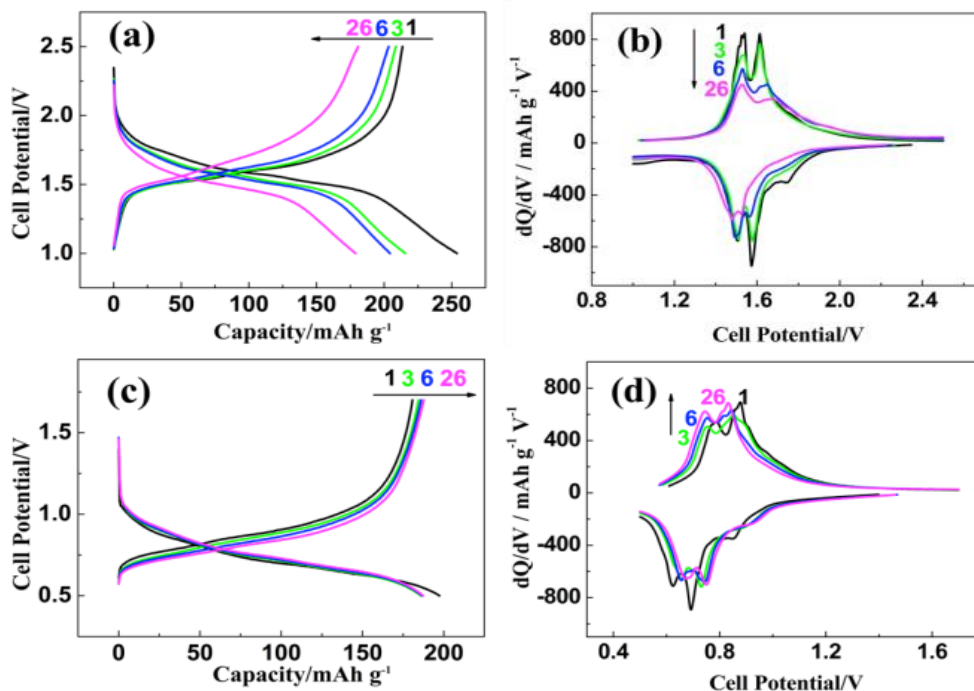
$TiO_2(B)|Li$ cells with 1.5 mol L^{-1} $LiBH_4/TG$ electrolyte show an S-shaped sloping voltage plateau on charge and discharge (Figure 2a) that is typical in the $TiO_2(B)$ system.[15, 16, 22] The first discharge and charge capacities are 254 mAh g^{-1} and 213.6 mAh g^{-1}, with an irreversible capacity loss (ICL) of 15.9%, which is likely caused by unwanted electrolyte degradation and irreversible trapping of Li^+.[14] The capacity observed above 1.7 V has been ascribed to either Li^+ insertion-deinsertion into $TiO_2(B)$ nanoflakes [15] or reactions between Li^+ and minor anatase TiO_2 [34]. We tend to agree with the former explanation, since anatase TiO_2 was not observed in the as-prepared $TiO_2(B)$. The incremental capacity in the range of 1.65-1.45 V corresponds to pseudo-capacitive Li^+ ion storage on the nanoflake surfaces, which is demonstrated in the differential capacity plots (Figure 2b). Upon cycling, the intercalation process becomes less obvious, while the pseudo-capacitive surface reaction becomes dominant, as evidenced by the increasing slopes. The capacitive capacity, however, gradually decreases during cycling, which may be due to the irreversible reaction of Li^+ ions with certain sites on the nanoflakes.

$TiO_2(B)|Mg$ cells with $Mg(BH_4)_2+LiBH_4/TG$ electrolyte show a plateau at approximately 0.7 V, lower than that for the $TiO_2(B)|Li$ cells (Figure 2c), which results from the standard potential difference between Mg metal and Li. The initial capacities are slightly lower than in the $TiO_2(B)|Li$ cells, which may be due to the lower ionic conductivity of the mixed Mg^{2+}/Li^+ electrolyte (535 µS cm^{-1}) compared with that of the single Li^+ electrolyte (603 µS cm^{-1}). The hybrid batteries, however, have much better efficiency, since the ICLs for the initial three cycles are 8.4%, 1.3%, and 0.8%, respectively. Considering the negligible capacity of the $TiO_2(B)|Mg$

cells with 0.5 mol L^{-1} $Mg(BH_4)_2$/TG electrolyte (Figure S3), the capacities of $TiO_2(B)|Mg$ cells with $Mg(BH_4)_2$+$LiBH_4$/TG electrolyte mainly come from reactions involving Li^+ ions. The location of the plateaus is evident in the differential capacity plots (Figure 2d). During cycling, the peak at approximately 0.85 V in the first cycle shifts towards higher potential and decreases in intensity, implying reduced Li^+ insertion-deinsertion; the peaks in the range of 0.8 - 0.5 V remain similar in intensity, indicative of steady pseudo-capacitive storage. The capacity in the low voltage region in the $TiO_2(B)|Mg$ cells with $Mg(BH_4)_2$+$LiBH_4$/TG electrolyte (63.3% and 68.9% capacitive contribution to the total storage for the 1st and 26th cycle, respectively) is larger compared with that of $TiO_2(B)|Li$ cells with $LiBH_4$/TG electrolyte (55.7% and 60.3% capacitive contribution for the 1st and 26th cycle, respectively) (shown in Figure 2b), suggesting a greater pseudo-capacitive contribution in the presence of Mg^{2+} ions.

The steady pseudo-capacitive contribution for the mixed $Mg(BH_4)_2$+$LiBH_4$/TG electrolyte, in contrast to the decreasing performance when only $LiBH_4$ was used, inspired us to find out if the Mg^{2+} ions participate in reactions during cycling. In other words, activation may be required for Mg^{2+} ions to be electrochemically active towards the $TiO_2(B)$ electrode. Figure S4 shows the discharge-charge curves of $TiO_2(B)|Mg$ cells with 0.5 mol L^{-1} $Mg(BH_4)_2$/TG electrolyte at 0.1 C. The $TiO_2(B)$ electrodes were respectively obtained by disassembling $TiO_2(B)|Li$ cells with $LiBH_4$/TG electrolyte, and $TiO_2(B)|Mg$ cells with $Mg(BH_4)_2$+$LiBH_4$/TG electrolyte after 26 cycles, and then carefully washing them in TG to remove the electrolyte salts. There are negligible capacities for the $TiO_2(B)|Mg(BH_4)_2$/TG|Mg cells, meaning that Mg^{2+} ions can neither be intercalated into $TiO_2(B)$ nor participate in any pseudo-capacitative reaction when only $Mg(BH_4)_2$ was used. These tests rule out the 'activation' of $TiO_2(B)$ so that it becomes electrochemically active towards Mg^{2+} ions. The *ex situ* XRD (Figure S5) and Raman patterns

(Figure S6) of TiO$_2$(B) at specific discharge and charge states show no noticeable difference when cycled in LiBH$_4$/TG and in Mg(BH$_4$)$_2$+LiBH$_4$/TG, respectively, which means that the capacity is predominantly from pseudo-capacitive reactions on the surface rather than the insertion reaction, which is consistent with the literature.[14]


Figure 2. (a) Discharge-charge profiles for selected cycles at 0.1 C (1 C = 335 mA g^{-1}) of the TiO$_2$(B)|Li cells with 1.5 mol L^{-1} LiBH$_4$/TG electrolyte, and (b) the corresponding differential capacity plots; (c) discharge-charge profiles for selected cycles of the TiO$_2$(B)|Mg cells with 0.5 mol L^{-1} Mg(BH$_4$)$_2$ + 1.5 mol L^{-1} LiBH$_4$/TG electrolyte, and (d) the corresponding differential capacity plots. The peak intensity in (d) levels off during cycling, indicating a steady contribution from the pseudo-capacitative reaction, in contrast to the degradation in (b), as evidenced by the decreasing peak intensity.

The effects of the electrolytes on the electrochemical performance of the 1D mesoporous TiO$_2$(B) nanoflakes was also investigated. Here, we used the optimal concentration considering the solubility and the performance. After 200 cycles, the TiO$_2$(B)|Li cells show a higher capacity of ~220 mAh g^{-1} in the electrolyte consisting of LiPF$_6$ in a mixture of ethylene carbonate and dimethyl carbonate (1:1 v/v) (LiPF$_6$/EC+DMC) (Figure S7a), while the cells with LiBH$_4$/TG electrolyte deliver ~150 mAh g^{-1} capacity and poor cycleability. This is in good agreement with reports that TiO$_2$(B) shows good cycleability in EC-based electrolyte, since the fluorine-containing salt suppresses surface reactions such as solvent decomposition.[35] Ester solvents passivate the Mg surface,[36] however, and Mg(PF$_6$)$_2$ fails to be a viable electrolyte salt for Mg batteies, so they can not be used to prepare mixed ion electrolyte for Mg^{2+}/Li$^+$ hybrid batteries. The TiO$_2$(B)|Mg cells deliever higher capacity and better cycling performance in Mg(BH$_4$)$_2$+LiBH$_4$/TG than in (PhMgCl)$_2$-AlCl$_3$+LiBH$_4$/THF (Figure S7b), which is likely to have resulted from better Mg deposition-disslution efficiency in Mg(BH$_4$)$_2$ based electrolyte (Figure S8).

Cyclic voltammetry (CV) was further used to explore the primary charge storage mechanism of TiO$_2$(B)|Mg in Mg(BH$_4$)$_2$+LiBH$_4$/TG electrolyte. For comparison, TiO$_2$(B)|Li cells in LiBH$_4$/TG electrolyte were also studied using CV. Three pairs of prominent cathodic/anodic peaks (Figure 3a) in the range of 1.4-1.95 V for TiO$_2$(B)|Li and 0.6-1.2 V for TiO$_2$(B)|Mg can be observed at a slow scan rate of 0.01 mV s^{-1}, which is consistent with the differential capacity curves (Figure 2b, d). The peak located at higher potential is denoted as B and two pairs at lower potentials are denoted as S2 and S1, respectively. For the TiO$_2$(B)|Li cells, the B peak is likely due to Li$^+$ insertion-deinsertion.[31] It should be noted that this peak sometimes was ascribed to the Li$^+$ ions interacting with minor anatase TiO$_2$,[37] which was not observed in our XRD and Raman

analysis (Figure 1a and 1b). The S2 and S1 peaks are related to the characteristic pseudo-capacitive behavior on the surface.[26] Similar reactions are observed in the $TiO_2(B)|Mg$ cells with $Mg(BH_4)_2$+LiBH$_4$/TG electrolyte. The peak currents for S2 and S1 scale with the first power of the scan rate (Figure 3d), indicating pseudo-capacitive reactions; the B peak scales with the square root of the scan rate (Figure 3c), which is related to ion insertion-deinsertion.[26] Compared with the $TiO_2(B)|Li$ cells, the $TiO_2(B)|Mg$ cells with $Mg(BH_4)_2$+LiBH$_4$/TG electrolyte show enhanced pseudo-capacitive behavior, as evidenced by the larger peak areas. At high scan rates, the peak current increments of S2 and S1 are much higher than that of B, which indicates that fast pseudo-capacitive ion transport occurring at the interface dominates the capacity.
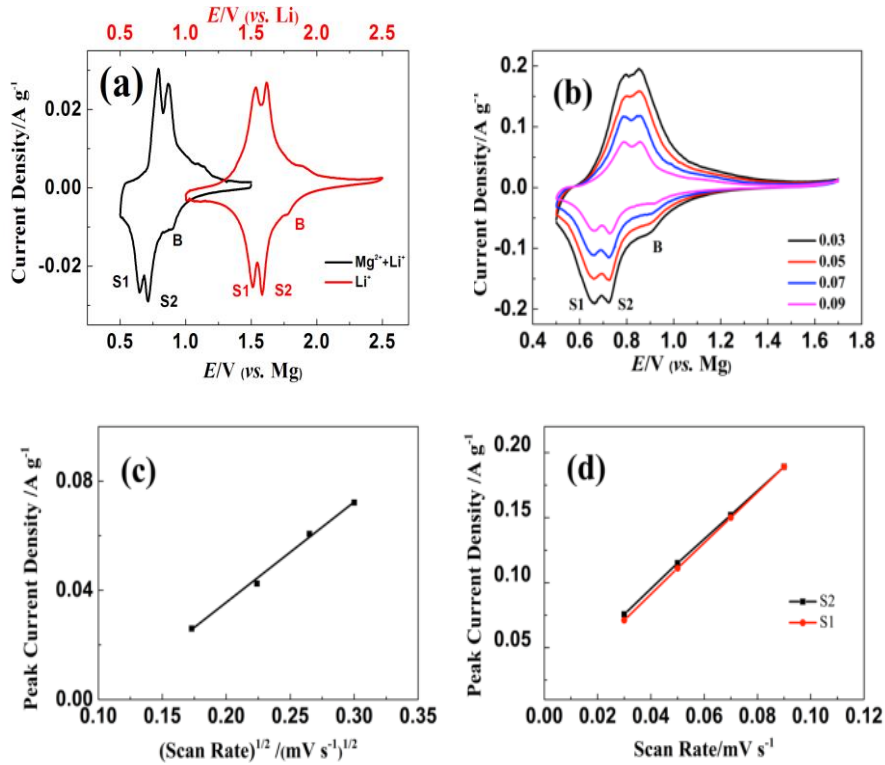
Figure 3. CVs of (a) $TiO_2(B)|Li$ cells with 1.5 mol L^{-1} LiBH$_4$/TG electrolyte and TiO_2 (B)|Mg cells with 0.5 mol L^{-1} $Mg(BH_4)_2$ + 1.5 mol L^{-1} LiBH$_4$/TG electrolyte at a scan rate of

0.01 mV S^{-1}, and (b) TiO$_2$(B)|Mg cells with 0.5 mol L^{-1} Mg(BH$_4$)$_2$ + 1.5 mol L^{-1} LiBH$_4$/TG electrolyte at different scan rates. For the TiO$_2$(B)|Mg cells, (c) B peak reduction currents scale with the square root of the scan rate, indicating ion insertion; (d) S2 and S1 peak reduction currents scale with the first power of the scan rate, indicating pseudo-capacitive reactions at the surface.
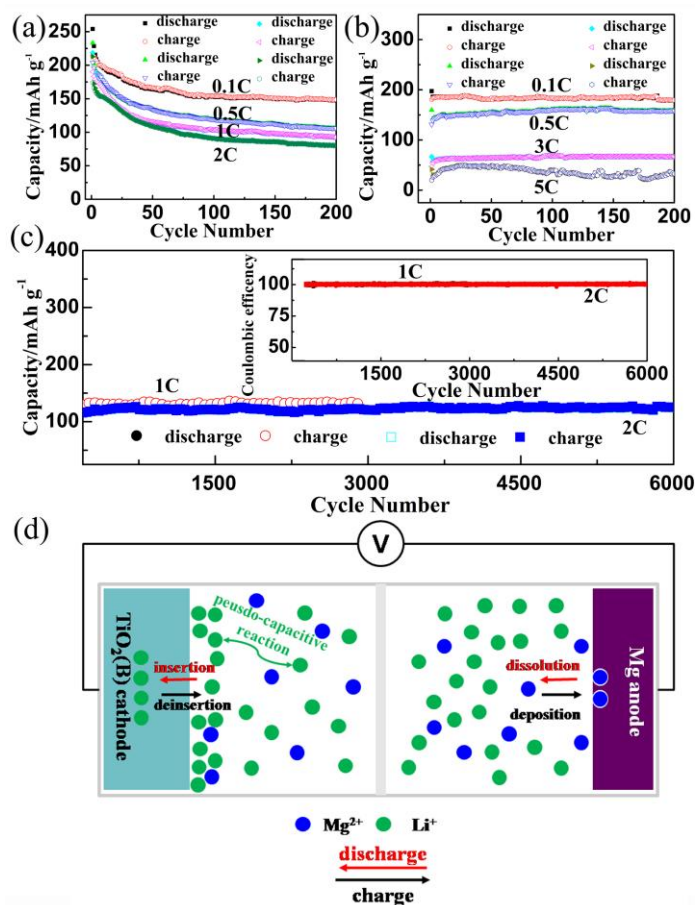
Figure 4. Rate capability of (a) TiO$_2$(B)|Li cells with 1.5 mol L^{-1} LiBH$_4$/TG electrolyte，(b) TiO$_2$(B)|Mg cells with 0.5 mol L^{-1} Mg(BH$_4$)$_2$ + 1.5 mol L^{-1} LiBH$_4$/TG electrolyte; (c) long-term cycling performance of the Mg^{2+}/Li$^+$ hybrid batteries at 1 and 2 C; (d) the proposed working mechanism of the Mg^{2+}/Li$^+$ hybrid battery.

Capacity degradation during cycling is a common feature of rechargeable batteries. High capacity retention with good coulombic efficiency will dramatically reduce operation costs. In our experiments, the hybrid batteries delivered exceptionally long-term (up to 6000 cycles) cycling performance, even at high rates (Figure 4a-4c). After 200 cycles, the hybrid batteries afford superior rate performance with 158.5 mAh g^{-1} at 0.5 C, 126.3 mAh g^{-1} at 1 C, and 115.6 mAh g^{-1} at 2 C, while LiBH$_4$/TG delivers only 105.5 mAh g^{-1} at 0.5 C, 92.7 mAh g^{-1} at 1 C, and 80.2 mAh g^{-1} at 2 C (Figure 4a, b, c). Hybrid cell and lithium cell showed similar capacity when cycled at a low rate of 0.2 mA cm^{-2}. However, for Li cell, a dramatic performance degradation was observed when the current was increased to 2 mA cm^{-2} due to Li dendrite formation.[10] Li metal is known to form dendrites that affect the electrochemical performance at high rate (>1 mA cm^{-2}).[38] This is unlikely in our tests due to the low current densities (0.1~5 C, 0.014~0.35 mA cm^{-2}). The hybrid cells demonstrate high capacity with good coulombic efficiency at high current rates of 1 C and 2 C up to 6000 cycles, with the capacity levelling off at about 115 mAh g^{-1} up to 6000 cycles at 2 C (Figure 4c).

The possible role of Mg^{2+} ions in this hybrid system can be considered from three aspects: insertion-deinsertion, pseudo-capacitive reactions on the surface, or 'catalytic activity' towards the reaction between Li$^+$ ions and TiO$_2$(B). Since TiO$_2$(B) shows no difference in its crystal structure (Figure S5) or Raman spectra (Figure S6) after cycling in both kinds of electrolyte, Mg^{2+} ions are unlikely to enter into the lattice. Furthermore, the discharge-charge curves, differential capacity plots (Figure 2), and CVs (Figure 3a, b), as well as the rate capability (Figure S9), indicate that the capacity of TiO$_2$(B) is largely associated with the pseudo-capacitive reactions at the surface. When the TiO$_2$(B) electrode was re-used (after cycling in two kinds of

electrolyte) to make TiO$_2$(B)|Mg(BH$_4$)$_2$/TG|Mg batteries, negligible capacity was observed (Figure S4). This finding indicates that Mg^{2+} ions alone will not contribute to the capacity of TiO$_2$(B) in either insertion-deinsertion or pseudo-capacitive reactions. Therefore, Mg^{2+} ions somehow contribute to the pseudo-capacitive reaction of Li$^+$ at the surface. Discovering if Mg^{2+} ions also participate in this reaction at the surface or just 'catalyse' the reaction between Li$^+$ and the TiO$_2$(B) surface is not possible at this stage. A safe conclusion is that the hybrid batteries are based on the pseudo-capacitive reaction dominated by a highly synergetic interaction between Li$^+$ and Mg^{2+}, and a likely mechanism is proposed in Figure 4d.

On the other hand, Li$^+$ ions are more 'reactive' when mixed with Mg^{2+} ions, which means that Li$^+$ ions become less constrained by counter BH$_4^-$ ions. In the ^{7}Li nuclear magnetic resonance (NMR) spectrum (Figure S10), LiBH$_4$ solution shows a resonance shift at -0.7 ppm, while in the Mg^{2+}/Li$^+$ solution, the signal shifts to -0.83 ppm, indicating increased electron shielding. The resultant higher electron cloud density around the Li$^+$ ions means stronger interaction between Li$^+$ ions and TG molecules (which have strong chelation arising from the five oxygen atoms per TG molecule), with consequently weakened Li$^+$ and BH$_4^-$ ion pair interaction and increased activity for Li$^+$ ions. It is not straightforward to accurately describe the dynamic interactions in solution between the Li$^+$ ions and the BH$_4^-$ and TG molecules upon adding Mg(BH$_4$)$_2$. Crystal structure analysis of LiBH$_4$ single crystals (with coordinated TG) grown from both kinds of electrolytes may shed some light, but so far we have not been successful in achieving the necessary single crystal for studies.

4. CONCLUSION

In this study, a high-performance Mg^{2+}/Li^+ hybrid battery with 1D mesoporous $TiO_2(B)$ nanoflakes as the cathode, Mg as the anode, and 0.5 mol L^{-1} $Mg(BH_4)_2$+1.5 mol L^{-1} $LiBH_4$/TG as the electrolyte has been developed. The batteries show a high charge capacity and good cycling performance with ~130 mAh g^{-1} at 1 C up to 3000 cycles and ~115 mAh g^{-1} at 2 C up to 6000 cycles. The capacity of these Mg^{2+}/Li^+ hybrid batteries is dominated by pseudo-capacitive reactions, and their efficiency is effectively enhanced by the presence of Mg^{2+} ions. The high specific capacity and cycle life at high rates, together with the intrinsic high safety of the Mg anode, make Mg^{2+}/Li^+ hybrid batteries a competitive candidate for electricity storage. Future work on the identification of mixed Mg^{2+}/Li^+ electrolyte with high anodic stability and efficient Mg deposition-dissolution, and of Li^+ ion active cathode with the optimum potential (relative to the electrolyte) would yield more effective Mg^{2+}/Li^+ hybrid batteries.

ASSOCIATED CONTENT

Supporting Information.

The anodic stability of $Mg(BH_4)_2$ + $LiBH_4$/TG, crystal structure of $TiO_2(B)$, discharge-charge curves of $TiO_2(B)$|Mg cells with 0.5 mol L^{-1} $Mg(BH_4)_2$/TG electrolyte, *Ex situ* XRD and Raman spectra patterns of $TiO_2(B)$, cycling performance and Coulombic efficiency, and NMR spectrum.

Corresponding Author

E-mail: nlyn@sjtu.edu.cn

E-mail: zhenguo@uow.edu.au.

Author Contributions

The manuscript was written through contributions of all authors. All authors have given approval to the final version of the manuscript.

Notes

The authors declare no competing financial interest.

REFERENCES

1. Aurbach, D.; Lu, Z.; Schechter, A.; Gofer, Y.; Gizbar, H.; Turgeman, R.; Cohen, Y.; Moshkovich, M.; Levi, E. Prototype Systems for Rechargeable Magnesium Batteries. *Nature* **2000**, *407*, 724–727.

2. Muldoon, J.; Bucur, C. B.; Oliver, A. G.; Sugimoto, T.; Matsui, M.; Kim, H. S.; Allred, G. D.; Zajicek, J.; Kotani, Y. Electrolyte Roadblocks to a Magnesium Rechargeable Battery. *Energy Environ. Sci*. **2012**, *5*, 5941–5950.

3. Knight, J. C.; Therese, S.; Manthiram, A. On the Utility of Spinel Oxide Hosts for Magnesium-Ion Batteries. *ACS Appl. Mater. Interfaces* **2015**, *7*, 22953–22961.

4. Choi, S. -H.; Kim, J.-S.; Woo, S.-G.; Sun, W. C.; Choi, Y.; Choi, J.; Lee, K.-T., Park, M.-S.; Kim, Y.-J. Role of Cu in Mo_6S_8 and Cu Mixture Cathodes for Magnesium Ion Batteries. *ACS Appl. Mater. Interfaces* **2015**, *7*, 7016–7024.

5. Gao, T.; Han, F. D.; Zhu, Y. J.; Suo, L. M.; Luo, C.; Xu, K.; Wang, C. S. Hybrid Mg^{2+}/Li^+ Battery with Long Cycle Life and High Rate Capability. *Adv. Energy Mater.* **2014**, *5*, 1401507.

6. Cheng, Y. W.; Shao, Y. Y.; Zhang, J. G.; Sprenkle, V. L.; Liu, J.; Li, G. S. High Performance Batteries Based on Hybrid Magnesium and Lithium Chemistry. *Chem. Commun.* **2014**, *50*, 9644–9646.

7. Yagi, S.; Ichitsubo, T.; Shirai, Y.; Yanai, S.; Doi, T.; Murase, K.; Matsubara, E. A Concept of Dual-salt Polyvalent-metal Storage Battery. *J. Mater. Chem. A* **2014**, *2*, 1144–1149.

8. Su, S. J.; Huang, Z. G.; NuLi, Y. N.; Tuerxun, F.; Yang, J.; Wang, J. L. A Novel Rechargeable Battery with a Magnesium Anode, a Titanium Dioxide Cathode, and a Magnesium Borohydride/tetraglyme Electrolyte. *Chem. Commun.* **2015**, *51*, 2641–2644.

9. Wu, N.; Yang, Z.-Z.; Yao, H.-R.; Yin, Y. X.; Gu, L.; Guo, Y.-G. Improving the Electrochemical Performance of the $Li_4Ti_5O_{12}$ Electrode in a Rechargeable Magnesium Battery by Lithium–Magnesium Co-Intercalation. *Angew. Chem., Int. Ed.* **2015**, *54*, 5757–5761.

10. Yoo, H. D.; Liang, Y. L.; Li, Y. F.; Yao, Y. High Areal Capacity Hybrid Magnesium−Lithium-Ion Battery with 99.9% Coulombic Efficiency for Large-Scale Energy Storage. *ACS Appl. Mater. Interfaces* **2015**, *7*, 7001−7007.

11. Tuerxun, F.; Abulizi, Y. S.; NuLi, Y. N.; Su, S. J.; Yang, J.; Wang, J. L. High Concentration Magnesium Borohydride/tetraglyme Electrolyte for Rechargeable Magnesium Batteries. *J. Power Sources* **2015**, *276*, 255–261.

12. Mohtadi, R.; Matsui, M.; Arthur, T. S.; Hwang, S. J. Magnesium Borohydride: From Hydrogen Storage to Magnesium Battery. *Angew. Chem., Int. Ed.* **2012**, *51*, 9780–9783.

13. Y. Y.; Shao, T. B.; Liu, G.; Li, S.; Gu, M.; Nie, Z. M.; Engelhard, M.; Xiao, J.; Lv, D. P.; Wang, C. M.; Zhang, J. G.; Liu, J. Coordination Chemistry in Magnesium Battery Electrolytes: How Ligands Affect Their Performance. *Sci. Rep.* **2013**, *3*, 3130.

14. Dylla, A. G.; Henkelman, G.; Stevenson, K. J. Lithium Insertion in Nanostructured TiO_2(B) Architectures. *Acc. Chem. Res.* **2013**, *46*, 1104–1112.

15. Ren, Y.; Liu, Z.; Pourpoint, F.; Armstrong, A. R.; Grey, C. P.; Bruce, P. G. Nanoparticulate TiO_2(B): An Anode for Lithium-Ion Batteries. *Angew. Chem., Int. Ed.* **2012**, *51*, 2164–2167.

16. Armstrong, A. R.; Armstrong, G.; Canales, J.; Bruce, P. G. TiO_2-B Nanowires. *Angew. Chem., Int. Ed.* **2004**, *43*, 2286–2288.

17. Armstrong, A. R.; Armstrong, G.; Canales, J.; Garcia, R.; Bruce, P. G. Lithium-Ion Intercalation into TiO_2-B Nanowires. *Adv. Mater.* **2005**, *17*, 862–865.

18. Li, J. M.; Wan, W.; Zhou, H. H.; Li, J. J.; Xu, D. S. Hydrothermal Synthesis of TiO_2(B) Nanowires with Ultrahigh Surface Area and Their Fast Charging and Discharging Properties in Li-ion Batteries. *Chem. Commun.* **2011**, *47*, 3439–3441.

19. Yang, Z. X.; Du, G. D.; Guo, Z. P.; Yu, X. B.; Chen, Z. X.; Guo, T. L.; Sharma, N.; Liu, H. H. TiO_2(B)@anatase Hybrid Nanowires with Highly Reversible Electrochemical Performance. *Electrochem. Commun.* **2011**, *13*, 46–49.

20. Armstrong, G.; Armstrong, A. R.; Canales, J.; Bruce, P. G. Nanotubes with the TiO_2-B Structure. *Chem. Commun.* **2005**, *19*, 2454–2456.

21. Shin, K.; Kim, H. J.; Choi, J.-M.; Choi, Y.-M.; Song, M. S.; Park, J. H. Controlled Synthesis of Skein Shaped TiO_2-B Nanotube Cluster Particles with Outstanding Rate Capability. *Chem. Commun.* **2013**, *49*, 2326–2328.

22. Myung, S.-T.; Takahashi, N.; Komaba, S.; Yoon, C. S.; Sun, Y.-K.; Amine, K.; Yashiro, H. Nanostructured TiO_2 and Its Application in Lithium-Ion Storage. *Adv. Funct. Mater.* **2011**, *21*, 3231–3241.

23. Huang, H.; Fang, J. W.; Xia, Y.; Tao, X. Y.; Gan, Y. P.; Du, J.; Zhu, W. J.; Zhang, W. K. Construction of Sheet-belt Hybrid Nanostructures from One-dimensional Mesoporous TiO_2(B) Nanobelts and Graphene Sheets for Advanced Lithium-ion batteries. *J. Mater. Chem. A* **2013**, *1*, 2495–2500.

24. Jiang, C. H.; Zhang, J. S. Nano Engineering Titania for High Rate Lithium Storage: A Review. *Sci. Technol.* **2013**, *29*, 97–122.

25. Guo, Y. G.; Hu, Y. Sh.; Sigle, W.; Maier J. Superior Electrode Performance of Nanostructured Mesoporous TiO_2 (Anatase) through Efficient Hierarchical Mixed Conducting Networks, *Adv. Mater.* **2007**, *19*, 2087–2091.

26. Liu, H. S.; Bi, Z. H.; Sun, X. G.; Unocic, R. R.; Paranthaman, M. P.; Dai, S.; Brown, G. M. Mesoporous TiO_2-B Microspheres with Superior Rate Performance for Lithium Ion Batteries. *Adv. Mater.* **2011**, *23*, 3450–3454.

27. Zhao, B.; Chen, F.; Liu, H. Q.; Zhang, J. L. Mesoporous TiO_2-B Nanowires Synthesized from Tetrabutyl Titanate. *J. Phys. Chem. Solids* **2011**, *72*, 201–206.

28. Furuya, Y.; Zhao, W. W.; Unno, M.; Noguchi, H. The Electrochemical Properties of Low-crystallinity TiO_2(B)-Carbon Composite as an Anode Material in Lithium Ion Battery. *Electrochim. Acta* **2014**, *136*, 266–273.

29. Qin, L.; Pan, X. X.; Wang, L.; Sun, X. P.; Zhang, G. L. X.; Guo, W. Facile Preparation of Mesoporous TiO_2(B) Nanowires with Well-dispersed Fe_2O_3 Nanoparticles and Their Photochemical Catalytic Behavior. *Appl. Catal., B* **2014**, *150–151*, 544–553.

30. Kobayashi, M.; Petrykin, V. V.; Kakihana, M. One-Step Synthesis of $TiO_2(B)$ Nanoparticles from a Water-Soluble Titanium Complex. *Chem. Mater.* **2007**, *19*, 5373–5376.

31. Aravindan, V.; Shubha, N.; Cheah, Y. L.; Prasanth, R.; Chuiling, W.; Prabhakar, R. R.; Madhavi, S. Extraordinary Long-term Cycleability of TiO_2-B Nanorods as Anodes in Full-Cell Assembly with Electrospun PVdF-HFP Membranes. *J. Mater. Chem. A* **2013**, *1*, 308–316.

32. Wang, J.; Zhou, Y. K.; Shao, Z. P. Porous $TiO_2(B)$/anatase Microspheres with Hierarchical Nano and Microstructures for High-Performance Lithium-ion batteries. *Electrochim. Acta* **2013**, *97*, 386–392.

33. Yamamoto, K.; Tomita, K.; Fujita, K.; Kobayashi, M.; Petrykin, V.; Kakihana, M. Synthesis of $TiO_2(B)$ Using Glycolato Titanium Complex and Post-Synthetic Hydrothermal Crystal Growth of $TiO_2(B)$. *J. Cryst. Growth* **2009**, *311*, 619–622.

34. Harada, Y.; Hoshina, K.; Inagaki, H.; Takami, N. Influence of Synthesis Conditions on Crystal Formation and Electrochemical Properties of $TiO_2(B)$ Particles as Anode Materials for Lithium-ion Batteries. *Electrochim. Acta* **2013**, *112*, 310–317.

35. Inaba, M.; Oba, Y.; Niina, F.; Murota, Y.; Ogino, Y.; Tasaka, A.; Hirota, K. $TiO_2(B)$ as a Promising High Potential Negative Electrode for Large-size Lithium-ion Batteries. *J. Power Sources* **2009**, *189*, 580–584.

36. Amir, N.; Vestfrid, Y.; Chusid, O.; Gofer, Y.; Aurbach, D. Progress in Nonaqueous Magnesium Electrochemistry. *J. Power Sources* **2007**, *174*, 1234–1240.

37. Li, X. L.; Zhang, Y. L.; Li, T. T.; Zhong, Q. E.; Li, H. Y.; Huang, J. M. Graphene Nanoscrolls Encapsulated $TiO_2(B)$ Nanowires for Lithium Storage. *J. Power Sources* **2014**, *268*, 372–378.

38. Aurbach, D.; Zinigrad, E.; Teller, H.; Dan, P. Factors Which Limit the Cycle Life of Rechargeable Lithium (Metal) Batteries. *J. Electrochem. Soc.* **2000**, *147*, 1274–1279.

Table of Contents Graphic